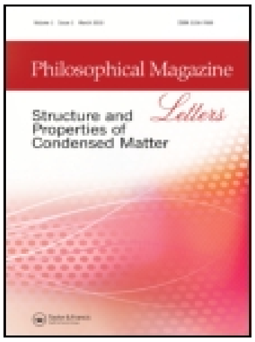

Philosophical Magazine Letters

ISSN: 0950-0839 (Print) 1362-3036 (Online) Journal homepage: http://www.tandfonline.com/loi/tphl20

Atomic imaging of the interface between $M_{23}C_6$-type carbide and matrix in a long-term ageing polycrystalline Ni-based superalloy

X.B. Hu, Y.L. Zhu, L.Z. Zhou, B. Wu & X.L. Ma

Philosophical Magazine Letters, 2015
Vol. 95, No. 4, 237–244, http://dx.doi.org/10.1080/09500839.2015.1039621

Taylor & Francis
Taylor & Francis Group

Atomic imaging of the interface between $M_{23}C_6$-type carbide and matrix in a long-term ageing polycrystalline Ni-based superalloy

X.B. Hu[a], Y.L. Zhu[a], L.Z. Zhou[b], B. Wu[a] and X.L. Ma[a]*

[a]*Shenyang National Laboratory for Materials Science, Institute of Metal Research, Chinese Academy of Sciences, Shenyang 110016, China;* [b]*Superalloys Division, Institute of Metal Research, Chinese Academy of Sciences, Wenhua Road 72, 110016 Shenyang, China*

(*Received 5 December 2014; accepted 2 April 2015*)

Besides the well-known cube-on-cube orientation relationship (OR) between $M_{23}C_6$ carbide and matrix, we have determined a new OR named as the twin-related OR in a long-term ageing Ni-based superalloy on the basis of the extensive and detailed electron diffraction analyses. Furthermore, by means of atomic-resolution high angle annular dark-field imaging technique which is implemented in the aberration-corrected scanning transmission electron microscope, we elucidated the interfacial characteristics between $M_{23}C_6$ and matrix for above two types of ORs. Taking into account of the interfacial characteristics, we propose that the twin-related OR possesses a higher total interfacial energy. Thus, its frequency of occurrence is lower than that of the cube-on-cube OR though both ORs are usually seen in the long-term ageing samples.

Keywords: Nickel-based superalloys; $M_{23}C_6$-type carbide; crystallographic orientation relationship

1. Introduction

Much attention has been paid to Nickel-based superalloys since they are widely used in the hot sections of aircraft engines and land-based gas turbines owing to their superior comprehensive properties at high temperature [1]. Due to the extremely aggressive service environment, performance as safety critical components is especially sensitive to the microstructural characteristics of materials. In most cases, microalloyed element of carbon is added into superalloys for purifying alloy melt, strengthening grain boundaries, and decreasing grain defects (freckle) formation. Consequently, precipitation of carbides in superalloys has been always inevitable, which is of great importance for getting the desired mechanical properties [2,3]. Thus, a systematic knowledge on the structural features of carbide is very crucial for a better understanding of the structure-related mechanical properties.

Among various types of carbide precipitated in the engineering alloy, $M_{23}C_6$ phase is a common one, where M represents transition metal atoms [4–11]. Meanwhile, it is well known that $M_{23}C_6$ usually precipitates in the γ/γ' matrix with the cube-on-cube orientation relationship (OR) [4,8,10]. Such an OR is known as unique between $M_{23}C_6$

*Corresponding author. Email: xlma@imr.ac.cn

and γ/γ' matrix, although any other crystallographic OR, if exists, is also of great importance. As for the interfacial characteristics between $M_{23}C_6$ and matrix, information shown in literature is relatively ambiguous. This is believed to result from the fact that the resolution of conventional transmission electron microscope (TEM) is rather limited. Atomic-scale information on the interfacial structure is necessary for elucidating the structure–property relationship [12–14]. It is also helpful for first-principles calculations and larger scale atomistic modelling. Fortunately, recent advance in aberration-corrected scanning TEM (STEM) enables structural analysis of an atomic scale [15–20]. In this study, we carry out detailed investigations on the OR and related interfacial characteristics between $M_{23}C_6$ phase and matrix by means of conventional as well as aberration-corrected STEMs.

2. Experimental procedure

The sample used in this study is a polycrystalline Ni-based superalloy with nominal composition (wt pct) of 15.5Cr-10.8Co-2.1Mo-5.6 W-3.2Al-4.6Ti-0.2Nb-0.4Hf-0.073C-0.075B-Ni balance. After produced in an industrial scale vacuum induction furnace, the master alloy was re-melted and casted into rods. Then the specimens were subjected to a standard heat treatment, 1170 °C/4 h/ air cool + 1050 °C/4 h air cool + 850 °C/16 h air cool. In order to elucidate the microstructural evolution, the standard heat-treated alloys were exposed at 900 °C for 10000 h. The electron transparent TEM foils were prepared by the routine mechanical thinning and Ar ion milling method.

Low magnification imaging and electron diffraction analyses were conducted on the JEM-2100 TEM operated at 200 kV. Atomic-resolution HAADF-STEM images were acquired on the Titan G^2 60-300 TEM equipped with a probe corrector, operated at 300 kV. The probe convergence semi-angle was approximate 25 mrad and the collection semi-angle of the HAADF detector ranged from 50 to 250 mrad. All the atomic-resolution HAADF images were processed by Wiener filter for removing the noise signal arising from amorphous layer at the surface of specimen [21–24]. The Fast Fourier transform patterns of the atomic images were used to determine the incident direction.

3. Results and discussion

As for the distribution of $M_{23}C_6$ carbide, besides precipitation along grain boundary (Figure 1a), grain interior precipitation is also popular (Figure 1d). In Figure 1a, the $M_{23}C_6$ grain possesses a definitive OR with grain I. Figure 1b is a composite electron diffraction patterns (EDPs) obtained from the region containing $M_{23}C_6$ and grain I. Diffraction spots with the highest intensity are reflection peaks of γ and the zone-axis can be labelled as $[0\ 0\ 1]_{\gamma}$. The pattern which is composed of the highest and the lowest intensity refection peaks results from γ' and the zone-axis can be indexed as $[0\ 0\ 1]_{\gamma'}$. In addition, the pattern composed of the highest and the medium intensity diffractions are from $M_{23}C_6$ phase with the zone-axis of $[0\ 0\ 1]_C$, where subscript C represents $M_{23}C_6$ carbide. These characteristics are schematically shown in Figure 1c which is a composite patterns of $[0\ 0\ 1]_M$ and $[0\ 0\ 1]_C$ with $(1\ 0\ 0)_M$ and $(1\ 0\ 0)_C$ plane parallel to each other, where subscript M represents matrix including γ and γ' phase. It is known

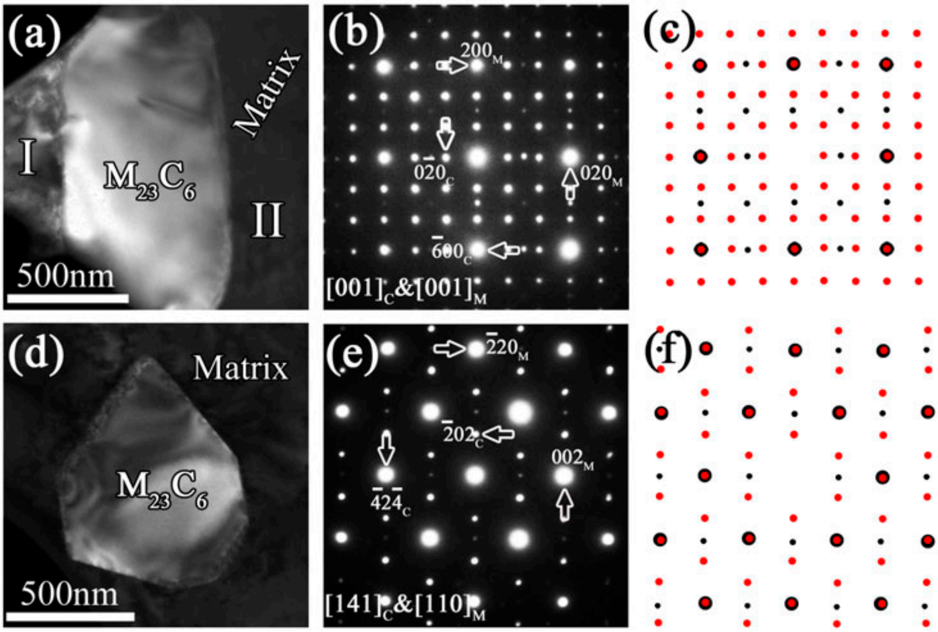

Figure 1. Dark-field (DF) image showing the $M_{23}C_6$ carbide precipitated (a) along grain boundary and (d) in grain interior. Two matrix grains in (a) are indicated by I and II. (b) Composite EDPs along $[0\ 0\ 1]_C//[0\ 0\ 1]_M$ zone-axis obtained from the region containing $M_{23}C_6$ and grain I. (e) Composite EDPs along $[1\ 4\ 1]_C//[1\ 1\ 0]_M$ zone-axis obtained from the region containing $M_{23}C_6$ and matrix. (c) and (f) schematic diagram corresponds to (b) and (e) composite EDPs, respectively, in which the transmission spots are omitted. Moreover, the black and red spots indicate the reflections originated from matrix and $M_{23}C_6$ carbide, respectively.

that $M_{23}C_6$ phase has a face-centred cubic structure with the space group of $Fm\bar{3}m$. Based on the presented EDPs, the lattice constant of $M_{23}C_6$ ($a = 1.08$ nm) is approximately three times than that of the matrix ($a = 0.36$ nm). This parallel relationship of $[0\ 0\ 1]_M//[0\ 0\ 1]_C$ and $[0\ 0\ 1]_M//[0\ 0\ 1]_C$ seen in Figure 1b is actually the well-known cube-on-cube OR. Apart from the cube-on-cube OR, an unusual crystallographic OR was also identified. The composite EDPs are displayed in Figure 1e, which was obtained from the area containing $M_{23}C_6$ and matrix as shown in Figure 1d. The diffraction pattern composed of the highest and the lowest intensity corresponds to the zone-axis of matrix with $[0\ 1\ 1]_M$ orientation. Based on the cube-on-cube OR, the corresponding zone-axis for $M_{23}C_6$ phase should also be $[0\ 1\ 1]_C$ zone-axis. However, this is unlikely true in Figure 1e, where the patterns with the highest and middle intensity correspond to $M_{23}C_6$ phase and the zone-axis can be indexed as $[1\ 4\ 1]_C$ direction. Therefore, this new OR with the parallel relationship of $(4\ \bar{2}\ 4)_C//(0\ 0\ 2)_M$ and $[1\ 4\ 1]_C//[1\ 1\ 0]_M$ are identified. The $(\bar{2}\ 0\ 2)_C$ and $(\bar{4}\ 2\ \bar{4})_C$ planes of $M_{23}C_6$ carbide are indicated with arrows. Figure 1e schematically illustrates these composite characteristics, where the superimposition of patterns of $[1\ 1\ 0]_M$ and $[1\ 4\ 1]_C$ with $(0\ 0\ 2)_M$ and $(4\ \bar{2}\ 4)_C$ parallel to each other is displayed.

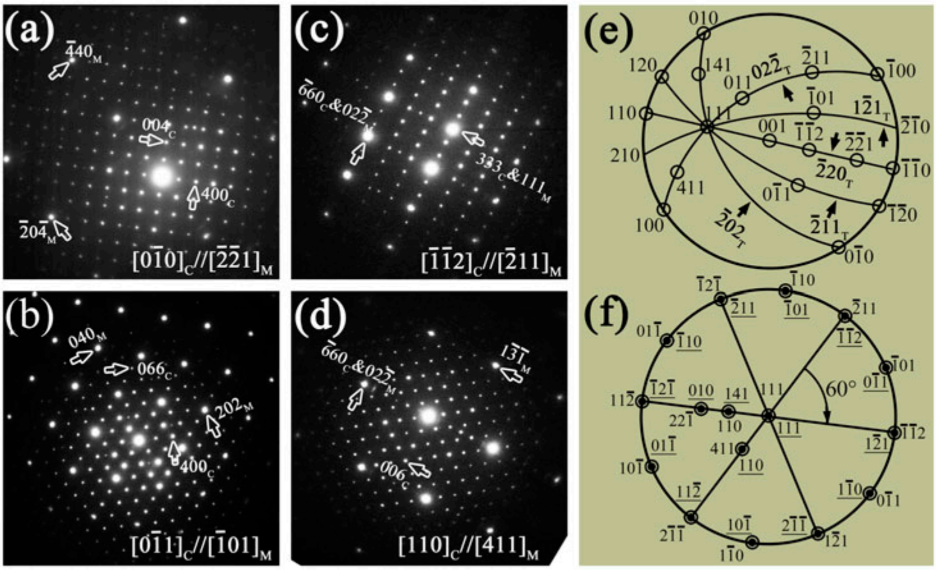

Figure 2. Composite EDPs between $M_{23}C_6$ and matrix along different zone-axes: (a) $[0\ \bar{1}\ 0]_C$// $[\bar{2}\ \bar{2}\ 1]_M$, (b) $[\bar{1}\ \bar{1}\ 2]_C$//$[\bar{2}\ 1\ 1]_M$, (c) $[0\ \bar{1}\ 1]_C$//$[\bar{1}\ 0\ 1]_M$ and (d) $[1\ 1\ 0]_C$//$[4\ 1\ 1]_M$. (e) The (0 0 1) stereographic projection describing the Guox analyses of EDPs displayed in Figures 1e and 2a–d, in which the $(\bar{2}\ 0\ 2)_T$, $(\bar{2}\ 2\ 0)_T$, $(0\ 2\ \bar{2})_T$, $(1\ \bar{2}\ 1)_T$, $(\bar{2}\ 1\ 1)_T$ denoted curves represent five traces of respective planes. (f) The (1 1 1) standard superimposed $M_{23}C_6$/matrix stereogram describing the twin-related crystallographic OR between $M_{23}C_6$ carbide and matrix (hkl: matrix, <u>hkl</u>: $M_{23}C_6$).

For further confirmation of this new OR between $M_{23}C_6$ phase and matrix, more composite EDPs are acquired as shown in Figure 2a–d which correspond to $[0\bar{1}0]_C$// $[\bar{2}\bar{2}1]_M$, $[\bar{1}\bar{1}2]_C$//$[\bar{2}11]_M$, $[0\bar{1}1]_C$//$[\bar{1}01]_M$ and $[1\ 1\ 0]_C$//$[4\ 1\ 1]_M$ zone-axis, respectively. We rationalize the collective rotation axis for $M_{23}C_6$ carbide and matrix by utilizing the method which was proposed by Goux for describing the relative orientations of single crystals [10,25,26]. Taken into account of the fact that the $[1\ 4\ 1]_C$ direction of $M_{23}C_6$ phase is parallel to $[1\ 1\ 0]_M$ direction of matrix as shown in Figure 1e, the collective rotation axis should be on a zone equidistant from $[1\ 4\ 1]_C$ of $M_{23}C_6$ and $[1\ 1\ 0]_M$ of matrix. This can be proposed that the collective rotation axis should be on a great circle that bisects the great circle through $[1\ 4\ 1]_C$ of $M_{23}C_6$ and $[1\ 1\ 0]_M$ of matrix. Meanwhile, based on the parallel planes shown in Figures 1e and 2a EDPs, we can construct the traces of $(\bar{2}\ 0\ 2)_T$ and $(\bar{2}\ 2\ 0)_T$ great circles in a (0 0 1) standard stereographic projection as shown in Figure 2e, where subscript T represents the trace. Then, the collective rotation axis should be on the bisecting great circle between $(\bar{2}\ 0\ 2)_T$ and $(\bar{2}\ 2\ 0)_T$, namely the $(\bar{2}\ 1\ 1)_T$ great circle with its trace shown in Figure 2e. Furthermore, according to the conjunct parallel plane shown in Figure 2c and d EDPs, we could construct the traces of $(0\ 2\ \bar{2})_T$ and $(\bar{2}\ 2\ 0)_T$. Thereby, another trace of $(1\ \bar{2}\ 1)_T$ great circle which contains the collective axis can be determined as shown in Figure 2e. Based on the combination of $(\bar{2}\ 1\ 1)_T$ and $(1\ \bar{2}\ 1)_T$ trace, the collective axis can be derived as [1 1 1].

Moreover, considering the intersection between $[0\ \bar{1}\ 1]$ and $[\bar{1}\ 0\ 1]$ which both contain the collective (1 1 1) plane as shown in Figure 2b, the rotation angle can be determined as 60°. In order to further clarify this OR, a superimposed stereogram is displayed in Figure 2f, where the normal of $M_{23}C_6$ and matrix are both [1 1 1] directions. It is clearly seen that through a rotation of 60° along [1 1 1] direction, the zone-axis of $[1\ 4\ 1]_C$, $[0\ 1\ 0]_C$, $[\bar{1}\ \bar{1}\ 2]_C$, $[0\ \bar{1}\ 1]_C$ and $[1\ 1\ 0]_C$ of $M_{23}C_6$ carbide would exactly coincide with that of $[1\ 1\ 0]_M$, $[2\ 2\ \bar{1}]_M$, $[\bar{2}\ 1\ 1]_M$, $[\bar{1}\ 0\ 1]_M$ and $[4\ 1\ 1]_M$, which are consistent with experimental observations. Considering the fact that rotating 60° along [1 1 1] zone-axis in a single phase of cubic system is actually a twin, we describe this new OR between $M_{23}C_6$ and matrix in terms of twin-related OR. According to above crystallographic analyses, this twin-related OR can be best stated as $[1\ 1\ 1]_C//[1\ 1\ 1]_M$, $[1\ \bar{1}\ 0]_C//[0\ \bar{1}\ 1]_M$ and $[\bar{1}\ \bar{1}\ 2]_C//[\bar{2}\ 1\ 1]_M$, which is similar to that of the OR between M_6C-type carbide precipitated in steels and the austenite matrix [27,28]. Additionally, with the help of above parallel relationships, it is convenient to introduce the matrix form adopted by Redjaimia [29] to express the new OR. This will be particularly helpful when any plane/direction from matrix is transformed to $M_{23}C_6$ carbide. The relationship between the planes (hkl) and the directions [uvw] in the two structures can be written as follows:

$$(\mathrm{hkl})_{M_{23}C_6}//M(\mathrm{hkl})_M \qquad (\mathrm{hkl})_M//M^{-1}(\mathrm{hkl})_{M_{23}C_6}$$

$$[\mathrm{uvw}]_M//M^t[\mathrm{uvw}]_{M_{23}C_6} \qquad [\mathrm{uvw}]_{M_{23}C_6}//(M^t)^{-1}[\mathrm{uvw}]_M.$$

The M is a basic matrix which transforms a plane in matrix to $M_{23}C_6$ carbide. The M^t and M^{-1} represent the transposed and inverse matrix of M, respectively. If we take into account the parallelism between the directions mentioned previously for the twin-related OR, we obtain the following matrix M:

$$M = \begin{pmatrix} 2 & -1 & 2 \\ 2 & 2 & -1 \\ -1 & 2 & 2 \end{pmatrix}.$$

To display the representative interfacial characteristic between $M_{23}C_6$ and matrix, atomic-resolution HAADF images are acquired as shown in Figure 3 for the cube-on-cube OR and Figure 4 for the twin-related OR. In Figure 3a and b, the matrix and $M_{23}C_6$ carbide are orientated along $[0\ 0\ 1]_{M/C}$ direction. It is evident that the connecting sharp interface consists of the low-index planes such as $(1\ 0\ 0)_{M/C}$ (Figure 3a) and $(1\ \bar{1}\ 0)_{M/C}$ (Figure 3b). Similarly, when the matrix and $M_{23}C_6$ carbide are tilted along $[1\ 1\ 0]_{M/C}$ orientation, we can also see the sharp interface with a low-index planes of $(1\ \bar{1}\ 1)_{M/C}$ (Figure 3c) and $(0\ 0\ 1)_{M/C}$ (Figure 3d). In addition, during our experimental observations, interfaces between $M_{23}C_6$ and matrix always possess the low-index planes such as $\{0\ 0\ 1\}_{M/C}$, $\{1\ 1\ 0\}_{M/C}$ and $\{1\ \bar{1}\ 1\}_{M/C}$ for the cube-on cube OR. Even when the interface seems high-index plane at a lower magnification, it is actually always constituted by above-mentioned low-index planes decorated with structural ledges in the atomic-resolution images. However, for the twin-related OR, the possible low-index connecting interface is only $(1\ 1\ 1)_{M/C}$ plane as shown in Figure 4, which is projected along $[0\ \bar{1}\ 1]_C//[\bar{1}\ 0\ 1]_M$ orientation. In other words, the option of low-index connecting

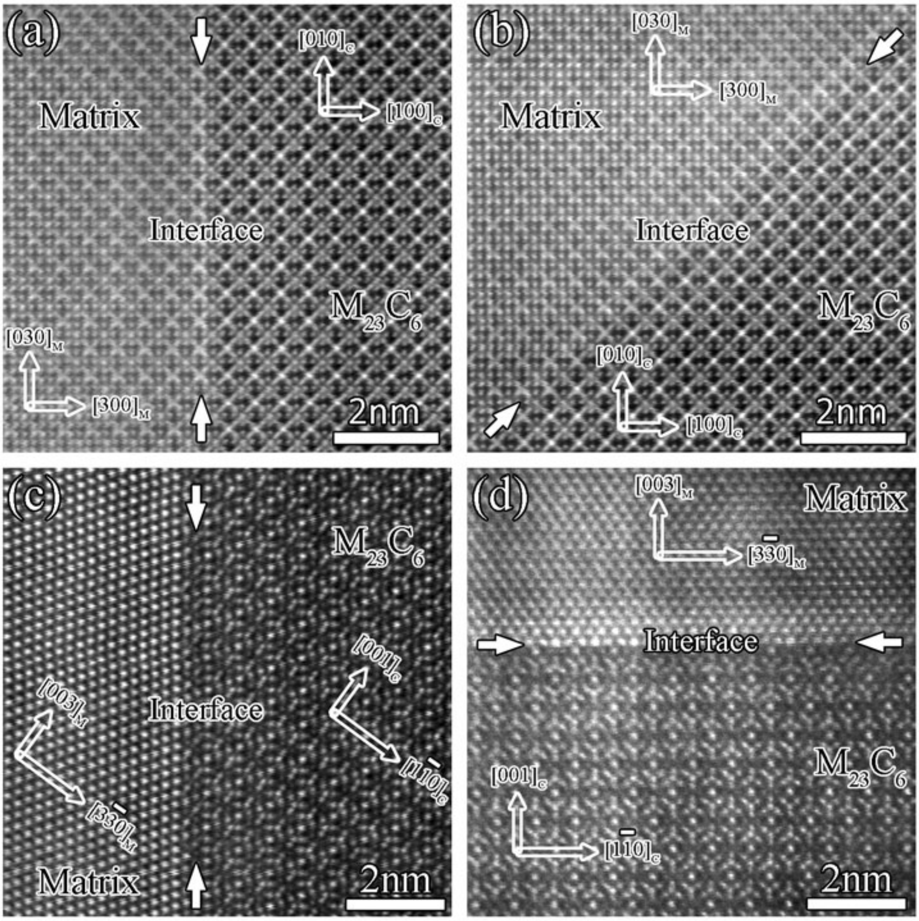

Figure 3. Atomic-resolution HAADF-STEM images viewed along (a), (b) $[0\ 0\ 1]_C//[0\ 0\ 1]_M$ and (c), (d) $[1\ 1\ 0]_C//[1\ 1\ 0]_M$ zone-axis displaying different interfacial types between $M_{23}C_6$ carbide and matrix with the cube-on-cube crystallographic OR. The crystallographic directions along the projected direction in $M_{23}C_6$ carbide and matrix, and location of the interface are all indicated.

planes between $M_{23}C_6$ and matrix for the twin-related OR is lower than that of the cube-on-cube OR. Based on above interfacial characteristics, we propose that the total interfacial energy for the cube-on-cube OR is lower than that of the twin-related OR because the low-index connecting interface always possesses a lower interfacial energy.

In the present TEM observations, the twin-related OR occasionally occurs, which implies that the interfacial energy is higher. We find more frequency of occurrence of the twin-related OR when the sample experienced longer time annealing at high temperatures. Nonetheless, the frequency of occurrence for the new twin-related OR is still lower than that of the cube-on-cube OR. A reasonable explanation is that the twin-related OR for the interface between $M_{23}C_6$ phase and matrix possesses a higher total interfacial energy as discussed above.

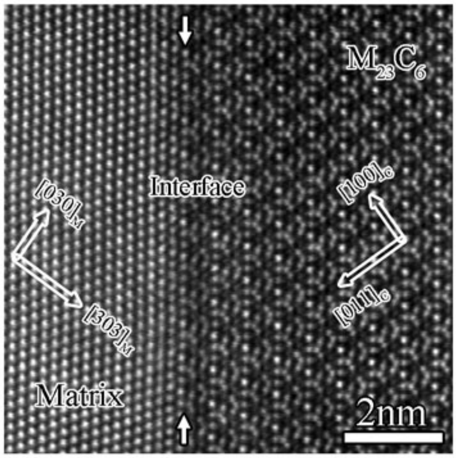

Figure 4. Atomic-resolution HAADF-STEM image projected along $[0\ \bar{1}\ 1]_C//[\bar{1}\ 0\ 1]_M$ zone-axis showing the interface between $M_{23}C_6$ carbide and matrix with the twin-related OR. The crystallographic directions along the projected direction in $M_{23}C_6$ carbide and matrix, and location of the interface are all indicated.

4. Conclusion

In summary, we report a systematic structural investigation on the OR between $M_{23}C_6$ and the matrix. Besides the well-known cube-on-cube OR, we have determined a new OR named as the twin-related OR with the parallel relationship of $[1\ 1\ 1]_C//[1\ 1\ 1]_M$, $[1\ \bar{1}\ 0]_C//[0\ \bar{1}\ 1]_M$ and $[\bar{1}\ \bar{1}\ 2]_C//[\bar{2}\ 1\ 1]_M$. Furthermore, we clarify that the connecting interface between $M_{23}C_6$ and matrix always possesses the configuration of low-index planes such as $\{0\ 0\ 1\}_{M/C}$, $\{1\ 1\ 0\}_{M/C}$ and $\{1\ \bar{1}\ 1\}_{M/C}$ as confirmed by atomic-resolution HAADF images. We propose that the total interfacial energy for twin-related OR be higher than that of cube-on-cube OR. This indirectly supports the experimental phenomenon that the frequency of occurrence for twin-related OR is still lower than that of cube-on-cube OR though both ORs occur in our long-term ageing samples.

Acknowledgements

The authors acknowledge the financial support from National Natural Foundation of China under 11327901 and National Basic Research Program of China under 2010CB631206 and 2009CB623705. And we are also grateful to J. Wang for bulk sample preparation.

Disclosure statement

No potential conflict of interest was reported by the authors.

Funding

This work was financially supported by the National Natural Foundation of China [grant number 11327901]; National Basic Research Program of China [grant number 2010CB631206], [grant number 2009CB623705].

References

[1] R.C. Reed (ed.), *The Superalloys: Fundamentals and Applications*, Cambridge University Press, Cambridge, 2006.
[2] L.Z. He, Q. Zheng, X.F. Sun, H.R. Guan, Z.Q. Hu, A.K. Tieu, C. Lu and H.T. Zhu, Mater. Sci. Eng. A 397 (2005) p.297.
[3] X.B. Hu, Y.B. Xue, S.J. Zheng, Y.L. Zhu, D. Chen and X.L. Ma, J. Alloy. Compd. 611 (2014) p.104.
[4] Y.H. Rong, Y.X. Guo and G.X. Hu, Metallography 22 (1989) p.47.
[5] G. Lvov, V. Levit and M. Kaufman, Metall. Mater. Trans. A 35 (2004) p.1669.
[6] L. He, Q. Zheng, X. Sun, G. Hou, H. Guan and Z. Hu, J. Mater. Sci. 40 (2005) p.2959.
[7] X.Z. Qin, J.T. Guo, C. Yuan, J.S. Hou and H.Q. Ye, Mater. Lett. 62 (2008) p.258.
[8] H.R. Zhang and O.A. Ojo, Philos. Mag. 90 (2010) p.765.
[9] M.H. Lewis and B. Hattersley, Acta Metall. 13 (1965) p.1159.
[10] T. Liu, S. Peng, Y. Lin and C. Wu, Metall. Mater. Trans. A 21 (1990) p.567.
[11] K. Kaneko, T. Fukunaga, K. Yamada, N. Nakada, M. Kikuchi, Z. Saghi, J.S. Barnard and P.A. Midgley, Scripta Mater. 65 (2011) p.509.
[12] R. Srinivasan, R. Banerjee, J.Y. Hwang, G.B. Viswanathan, J. Tiley, D.M. Dimiduk and H.L. Fraser, Phys. Rev. Lett. 102 (2009) p.086101.
[13] L. Bourgeois, C. Dwyer, M. Weyland, J.F. Nie and B.C. Muddle, Acta Mater. 59 (2011) p.7043.
[14] S. Sanyal, U.V. Waghmare, T. Hanlon and E.L. Hall, Mater. Sci. Eng. A 530 (2011) p.373.
[15] J.F. Nie, Y.M. Zhu, J.Z. Liu and X.Y. Fang, Science 340 (2013) p.957.
[16] Z.Q. Yang, M.F. Chisholm, G. Duscher, X.L. Ma and S.J. Pennycook, Acta Mater. 61 (2013) p.350.
[17] S. Wenner, C.D. Marioara, Q.M. Ramasse, D.-M. Kepaptsoglou, F.S. Hage and R. Holmestad, Scripta Mater. 74 (2014) p.92.
[18] J.M. Rosalie, C. Dwyer and L. Bourgeois, Acta Mater. 69 (2014) p.224.
[19] M. Fiawoo, X. Gao, L. Bourgeois, N. Parson, X.Q. Zhang, M. Couper and J.F. Nie, Scripta Mater. 88 (2014) p.53.
[20] X.B. Hu, Y.L. Zhu, N.C. Sheng and X.L. Ma, Sci. Rep. 4 (2014) p.7367.
[21] R. Kilaas, J Microsc. 190 (1998) p.45.
[22] P. Donnadieu, Y. Shao, F. De Geuser, G.A. Botton, S. Lazar, M. Cheynet, M. de Boissieu and A. Deschamps, Acta Mater. 59 (2011) p.462.
[23] S. Lay and J.M. Missiaen, Philos. Mag. 93 (2013) p.1146.
[24] X.B. Hu, Y.L. Zhu and X.L. Ma, Acta Mater. 68 (2014) p.70.
[25] C. Goux, Bull. Cercle d'Etudes Metaux 8 (1961) p.185.
[26] P.H. Pumphrey and K.M. Bowkett, Scripta Metall. 5 (1971) p.365.
[27] S. Peng, T. Tsai and C. Chou, Metall. Mater. Trans. A 24 (1993) p.1671.
[28] S.W. Peng and C.P. Chou, Scripta Metall. Mater. 26 (1992) p.243.
[29] A. Redjaïmia, J. Morniroli, P. Donnadieu and G. Metauer, J. Mater. Sci. 37 (2002) p.4079.